Citation: CPT Pharmacometrics Syst. Pharmacol. (2020) 9, 48–59; doi:10.1002/psp4.12482

ARTICLE

Integrated Two-Analyte Population Pharmacokinetic Model of Polatuzumab Vedotin in Patients With Non-Hodgkin Lymphoma

Dan Lu[1,*,†], Tong Lu[1,*,†], Leonid Gibiansky[2], Xiaobin Li[1], Chunze Li[1], Priya Agarwal[1], Colby S. Shemesh[1], Rong Shi[1], Randall C. Dere[1], Jamie Hirata[1], Dale Miles[1], Pascal Chanu[3], Sandhya Girish[1] and Jin Yan Jin[1]

A two-analyte integrated population pharmacokinetic (PK) model that simultaneously describes concentrations of antibody-conjugated monomethyl auristatin E (acMMAE) and unconjugated MMAE following repeated administrations of polatuzumab vedotin (pola) was developed based on data from four clinical studies of pola in patients with non-Hodgkin lymphoma. A two-compartment model with a nonspecific, time-dependent linear clearance, a linear time-dependent exponentially declining clearance, and a Michaelis–Menten clearance provided a good fit of the acMMAE plasma PK profiles. All three acMMAE elimination pathways contributed to the input to the central compartment of unconjugated MMAE, which was also described by a two-compartment model. Population PK parameters, covariate effects, and interindividual variability of model parameters were estimated. The impact of clinically relevant covariates on PK exposures of each analyte were quantified and reported to support key label claims.

Study Highlights

WHAT IS THE CURRENT KNOWLEDGE ON THE TOPIC?

☑ Population pharmacokinetic (popPK) modeling of antibody-conjugated monomethyl auristatin E (acMMAE) alone showed that acMMAE exposure correlates with efficacy and safety after polatuzumab vedotin (pola) treatment in patients with non-Hodgkin lymphoma. However, incorporating the key catabolite unconjugated monomethyl auristatin E (MMAE) to the model is important.

WHAT QUESTION DID THIS STUDY ADDRESS?

☑ A two-analyte integrated popPK model was developed to simultaneously describe acMMAE and unconjugated MMAE pharmacokinetics (PK) following repeated treatment.

WHAT DOES THIS STUDY ADD TO OUR KNOWLEDGE?

☑ This semimechanistic model, which overall is aligned with hypothetical antibody–drug conjugate (ADC) disposition mechanisms, identified three clearance pathways of acMMAE, with nonspecific clearance playing a major role. Consequently, there are three input rates for MMAE formation that change over time. The impact of clinically relevant baseline covariates on PK exposures of both acMMAE and MMAE were quantified.

HOW MIGHT THIS CHANGE CLINICAL PHARMACOLOGY OR TRANSLATIONAL SCIENCE?

☑ The model supports key clinical pharmacology-related label claims for pola and provides a modeling framework for ADC PK analysis.

Polatuzumab vedotin (pola) is a cluster of differentiation 79b (CD79b)-directed antibody–drug conjugate (ADC) with activity against proliferating B cells.[1] The small molecule, monomethyl auristatin E (MMAE), an antimitotic agent with a mechanism of action similar to vincristine but 100–1,000 times more potent,[2] is covalently attached to the antibody via a protease-cleavable linker.[1,3] The antibody binds to CD79b, a B-cell-specific surface protein and signaling component of the B-cell receptor, which is expressed ubiquitously across most mature B-cell lymphomas.[4] Upon binding CD79b, pola is internalized, and the linker is cleaved to enable intracellular delivery of MMAE.[5] MMAE binds to microtubules and kills dividing cells by inhibiting cell division and inducing apoptosis.[6]

Pola has shown promising efficacy and an acceptable safety profile in phase I/II clinical trials in non-Hodgkin lymphoma (NHL).[7–12] Combination of pola with bendamustine (B) and rituximab (R) at the recommended dose of 1.8 mg/kg once every 3 weeks (q3w) for up to six cycles demonstrated enhanced efficacy (median overall survival increased from 4.7 to 12.4 months) in relapsed/refractory (R/R) diffuse large B-cell lymphoma (DLBCL) when

†Equal contributions.

[1]Genentech Inc., South San Francisco, California, USA; [2]QuantPharm LLC, North Potomac, Maryland, USA; [3]Genentech/Roche, Lyon, France. *Correspondence: Dan Lu (lu.dan@gene.com) and Tong Lu (lu.tong@gene.com)

Received: August 12, 2019; accepted: November 3, 2019. doi:10.1002/psp4.12482

compared with B and R alone[13,14] and was approved in the United States for the treatment of R/R DLBCL after at least two prior therapies.[14]

The pharmacokinetics (PK) of ADCs consider the large-molecule and small-molecule components.[15–17] Three analytes are routinely measured in clinical trials: total antibody (Tab), antibody-conjugated MMAE (acMMAE), and unconjugated MMAE.[18,19] Based on noncompartmental analyses (NCA) after the first dose, the plasma exposure of acMMAE and unconjugated MMAE increased proportionally over the dose range 0.1–2.4 mg/kg.[7] PK exposures of acMMAE positively correlate with objective response rate and with grade 2 peripheral neuropathy,[20] and unconjugated MMAE, a highly potent catabolite, may correlate with safety outcome. In this study, we report the development of a two-analyte acMMAE–MMAE population PK (popPK) model with covariate assessment on each analyte, to support regulatory filing. A two-analyte integrated popPK model describing the clinical PK of Tab and acMMAE of two ADCs (pola and pinatuzumab vedotin)[15] was developed but did not include unconjugated MMAE. A three-analyte integrated model (Tab–acMMAE–MMAE) was explored but was thought to provide limited added value for the regulatory filing.

METHODS

Study design and data

The popPK model was based on data from four clinical studies of pola 0.1–2.4 mg/kg as monotherapy or in combination regimens in patients with NHL (phase I/Ib DCS4968g (NCT01290549), phase Ib/II GO27834 (NCT01691898, ROMULUS), phase Ib/II GO29365 (NCT02257567), phase Ib/II GO29044 (NCT01992653; **Table S1**).[7–12] Pola was administered as a mixture of drug-to-antibody ratio (DAR) species ranging from 0–8, with a mean DAR of 3.65 (Genentech data on file). Studies were approved by the medical ethics committee and carried out in accordance with the International Conference on Harmonization guidelines for Good Clinical Practice. A relatively intensive PK sampling (**Table S1**) was used for the single-agent DCS4968g study (>30 plasma samples/patient across multiple cycles), to help define the model structure. For the other studies, less-intensive PK sampling was performed.

Bioanalytical methods

A validated immunoaffinity liquid chromatography method detected by tandem mass spectrometry was developed to measure acMMAE (total MMAE conjugated to the antibody) concentrations in human plasma, with a lower limit of quantitation of 0.359 ng/mL (0.50 nM) MMAE. A validated protein precipitation/liquid chromatography method, detected by tandem mass spectrometry, determined unconjugated MMAE concentrations, with a lower limit of quantitation of 0.0359 ng/mL (0.05 nM) unconjugated MMAE.

Modeling methods

The dose of acMMAE in the popPK data set was converted to MMAE equivalent dose in μg, which equates to:

$$3.65 \times \frac{718}{145{,}001} \times \text{pola dose in } \mu\text{g/ kg} \times \text{body weight in kg}$$

where mean DAR = 3.65, molecular weight (Daltons) for unconjugated MMAE = 718, and molecular weight of the antibody-drug conjugate = 145,001.

The popPK analysis was conducted via nonlinear mixed-effects modeling with Nonlinear Mixed-Effect Modeling (NONMEM) software, version 7.3.0 (ICON Development Solutions, Ellicott City, MD), using the first-order conditional estimation method with eta-epsilon interaction. Graphical and all other statistical analyses, including the evaluation of NONMEM outputs, were performed using R version 3.3.3.[21]

The integrated acMMAE–MMAE popPK model was developed sequentially in four steps. For each step, the model that best described the observed data was determined by overall goodness-of-fit (GOF) measures, including GOF plots, prediction-corrected visual predictive check,[22] normalized prediction distribution error (NPDE) plots,[23,24] and objective function value.

First (step 1), the base acMMAE popPK model (without covariates) was developed and modified on the basis of historical model structures for ADCs but with innovations to best describe pola data.[15–17] The popPK of acMMAE reported here was described by a two-compartmental model with three clearance pathways as described in the Results section.

Second (step 2), the integrated acMMAE–MMAE base model was developed by simultaneously fitting acMMAE and unconjugated MMAE PK data, starting from the base acMMAE PK model from step 1 to infer the MMAE formation and elimination kinetics. A two-compartment model of unconjugated MMAE with linear elimination was first used and the addition of Michaelis–Menten (MM) elimination further improved estimation at low concentrations. Each of the three acMMAE clearance pathways contributed to unconjugated MMAE formation. Further improvement of the fit was achieved when the acMMAE to unconjugated MMAE conversion fraction relative to each of the three acMMAE elimination pathways was allowed to be different and by including a time-dependent decrease in the same rate for all three conversion fractions.

Third (step 3), using a variation of the full-model approach,[25,26] the covariate model for acMMAE was developed starting with inclusion of all predefined covariates (**Table S2**) to the base acMMAE model (step 1). Predefined covariates were selected based on prior experience with monoclonal antibodies (mAbs), B-cell target-mediated disposition, and factors of clinical interest related to demographics, disease, line of therapy, combination drugs and organ functions.

Lastly (step 4), the integrated covariate model for acMMAE–MMAE (final model) was developed by identifying covariates for unconjugated MMAE, which led to the reduction of the interindividual variability (IIV) of MMAE PK parameters in addition to those identified for acMMAE in step 3. All covariate effects for the unconjugated MMAE model were applied to the fractions of formation (same effects for all three pathways of acMMAE to unconjugated MMAE conversion), as the model cannot distinguish between covariate effects on the systemic PK parameters of unconjugated MMAE (e.g., apparent clearance, apparent volume of distribution) and covariate effects on acMMAE to unconjugated MMAE relative fractions of formation. The

covariates included predefined covariates of interest similar to those assessed for acMMAE and additional covariates that may be unique for unconjugated MMAE.

In steps 3 and 4, strongly correlated covariates were not all included in the model (on the same parameter). To arrive at a parsimonious model, covariate effects with 95% confidence intervals (CIs) that included the null value were removed if the associated change of objective function value was not significant at 0.01 level (e.g., the effect of age on unconjugated MMAE conversion fraction). Additional covariates identified by the diagnostic plots were added (e.g., the effect of Asian race on central volume for acMMAE, the effect of albumin on unconjugated MMAE conversion fraction).

Sensitivity analysis

A sensitivity analysis, based on the final integrated acMMAE–MMAE model, was performed to assess the magnitude of impact of each covariate on PK exposures (area under the concentration-time curve (AUC) and maximum concentration (C_{max}) at cycle 6 following 1.8 mg/kg q3w). For continuous covariates, the simulated exposures at the 2.5th and 97.5th percentiles of each covariate (with other covariates fixed at the reference value) were compared with the exposures for a typical patient with all covariates fixed at the reference value. For categorical covariates, the simulated exposures at one category were compared with the reference category.

RESULTS

acMMAE–MMAE integrated final model

Data from 460 patients with NHL from the four pola clinical studies are reported (**Table S1**) and include 4,215 acMMAE and 4,194 unconjugated MMAE time–concentration pairs. All data collected with a time after the most recent dose of >6 weeks (1,008 hours) were excluded from analysis given that these data may not be clinically relevant in the context of the regimens tested in the clinical setting (i.e., q3w and every 4 weeks). All post-first-dose below-limit-of-quantification data including 215 (4.5%) acMMAE and 434 (9.2%) unconjugated MMAE data were excluded from the analysis. Among them, 93 acMMAE and 135 unconjugated MMAE values were collected within the time after the most recent dose of 1,008 hours. The M3 method[27,28] was not applied to the final model given the low percentage of below-limit-of-quantification data. An exploration using the M3 method confirmed a lack of impact on the parameter estimations.

The final model described the PK of acMMAE and unconjugated MMAE simultaneously (**Figure 1**). Estimates of structural fixed-effect, covariate fixed-effect, and random-effects parameters for the final integrated model are listed in **Tables 1 and 2**; **Table S3**, respectively. All model parameters were estimated with good precision, confirming that the observed data were sufficient to identify all model parameters in this relatively complex model. The prediction-corrected visual predictive check and GOF

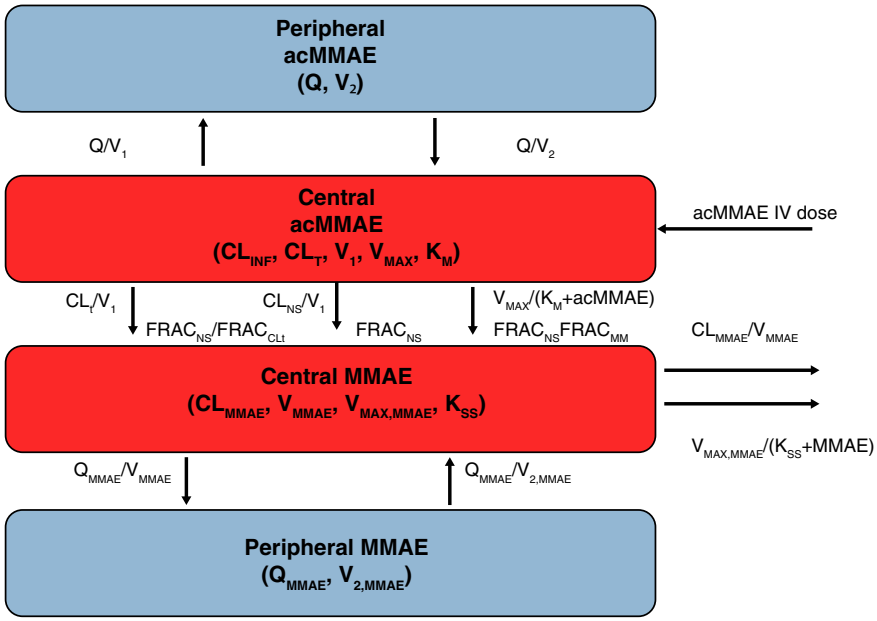

Figure 1 Schematic representation of the structural acMMAE–MMAE model. $CL_{NS} = CL_{INF} \cdot (1 + CL_{INF,EMAX} \cdot T_{50}^{\gamma} / (T_{50}^{\gamma} + t^{\gamma}))$: acMMAE nonspecific clearance (t in months); $CL_t = CL_T \cdot \exp(-k_{des} \cdot t)$ (t in hours). ac, antibody-conjugated; CL, clearance; CL_{NS}, nonspecific time dependent clearance; CL_{INF}, CL_{NS} at time of infinity; CL_{INF}, acMMAE nonspecific linear clearance at time of infinity; CL_{MMAE}, unconjugated MMAE apparent clearance; $FRAC_{NS}$, acMMAE-unconjugated MMAE relative conversion fraction for nonspecific elimination; $FRAC_{CLT}$, ratio of acMMAE-unconjugated MMAE conversion fractions for CL_t and CL_{NS} elimination pathways; $FRAC_{MM}$, ratio of acMMAE-unconjugated MMAE conversion fractions for Michaelis–Menten and CL_{NS} elimination pathways; IV, intravenous; K_M, Michaelis–Menten constant of acMMAE elimination; K_{SS}, Michaelis–Menten constant of unconjugated MMAE elimination; MMAE, monomethyl auristatin E; Q, acMMAE intercompartment clearance; V_1, acMMAE central volume; V_2, acMMAE peripheral volume; V_{max}, maximum acMMAE Michaelis–Menten elimination rate; Q_{MMAE}, unconjugated MMAE apparent inter-compartment clearance; V, volume; V_{MMAE}, unconjugated MMAE apparent central volume; $V_{2,MMAE}$, unconjugated MMAE peripheral volume; $V_{max,MMAE}$, maximum unconjugated MMAE Michaelis–Menten elimination rate.

Table 1 Estimates of structural fixed-effect parameters for the final integrated model

Parameter		Definition	Value	RSE%	95% CI
acMMAE parameters					
k_{des} (1/hour)	θ_1	Rate constant of CL_t decrease	0.0046	7.95	0.00389–0.00532
CL_T (L/hour)	θ_2	Initial time-dependent CL	0.00623	19.6	0.00383–0.00862
CL_{INF} (L/hour)	θ_3	Nonspecific linear clearance after repeated dosing	0.0344	3.6	0.032–0.0368
V_1 (L)	θ_4	Central volume	3.15	1.58	3.05–3.25
V_2 (L)	θ_5	Peripheral volume	3.98	2.92	3.75–4.2
Q (L/hour)	θ_6	Intercompartment rate	0.0145	2.53	0.0138–0.0153
V_{max} (ng/mL/hour)	θ_7	Maximum MM elimination	0.0203	14.3	0.0146–0.026
K_M (ng/mL)	θ_8	MM constant	0.604	36.2	0.175–1.03
$CL_{INF,MAX}$	θ_9	Maximum effect of time on CL_{NS}	0.223	8.6	0.185–0.261
T_{50} (month)	θ_{10}	Time of the half-effect of $CL_{INF,MAX}$	3.53	6.77	3.07–4
γ	θ_{11}	Sigmoidicity of $CL_{NS}(t)$ function	2.27	12.5	1.71–2.82
Unconjugated MMAE parameters					
V_{MMAE} (L)	θ_{12}	Unconjugated MMAE apparent central volume	82.2	8.15	69.1–95.4
CL_{MMAE} (L/hour)	θ_{13}	Unconjugated MMAE apparent clearance	1.89	8.14	1.59–2.2
Q_{MMAE} (L/hour)	θ_{14}	Unconjugated MMAE apparent inter-compartment clearance	36.3	12.3	27.5–45.1
$V_{2,MMAE}$ (L)	θ_{15}	Unconjugated MMAE apparent peripheral volume	200	6.13	176–224
$V_{MAX,MMAE}$ (ng/mL/hour)	θ_{16}	Maximum MM elimination	0.0307	9.17	0.0252–0.0362
K_{SS} (ng/mL)	θ_{17}	MM constant	0.581	10.5	0.461–0.701
$FRAC_{CLT}$	θ_{18}	Factor for relative conversion fraction of CL_t pathway	3.70	3.11	3.48–3.93
$FRAC_{MM}$	θ_{19}	Factor for relative conversion fraction of MM pathway	2.72	9.45	2.21–3.22
ALPH (1/month)	θ_{20}	Rate constant of $FRAC_T$ decrease	0.167	38.5	0.0411–0.293
$FRAC_T$	θ_{21}	Initial time-dependent part of $FRAC_{NS}$	0.139	21.0	0.0816–0.196

ac, antibody-conjugated; CI, confidence interval; CL, clearance; $FRAC_{NS}$, relative conversion fraction for nonspecific elimination; MM, Michaelis–Menten; MMAE, monomethyl auristatin E; PE, parameter estimate; RSE%, relative standard error (i.e., 100·SE/PE); SE, standard error. θ_1 to θ_{21} symbols indicate fixed-effects parameters of the final model.

plots showed good agreement between simulated and observed data (**Figures S1 and S2**). The NPDE plots also showed good predictive abilities of the model, with no strong dependencies of NPDE on time, time after dose, population predictions, nominal dose, histology, or study (**Figure S3**).

PopPK of acMMAE

Both the acMMAE alone (model development step 3) and integrated acMMAE–MMAE final model (model development step 4) described the observed acMMAE PK data well with comparable population and individual predictions, indicating that simultaneous fitting of the catabolite (MMAE) and parent (acMMAE) did not impact the fitting of the parent (Genentech, data on file). The acMMAE PK model is a two-compartmental model. Three clearance pathways, i.e., nonspecific time-dependent linear clearance (CL_{NS}), linear time-dependent exponentially declining clearance (CL_t), and MM clearance (CL_{MM}), were identified to describe the data. All three clearance values, as plotted by a typical patient upon pola 1.8 mg/kg q3w dosing, change over time with CL_{NS} contributing to the majority of the totals clearance (**Figure 2a**).

The CL_{NS} declined slowly with time, as modeled by the Hill function (Eq. 1).

$$CL_{NS} = CL_{INF} \cdot \left(1 + CL_{INF,EMAX} \times \frac{T_{50}^{\gamma}}{T_{50}^{\gamma} + time^{\gamma}}\right) \quad (1)$$

where CL_{INF}: nonspecific linear clearance at infinity after hypothetical repeated q3w dosing, $CL_{INF,EMAX}$: maximum effect of time on CL_{NS}, T_{50}: time to half-maximal effect, and γ = Hill coefficient.

Table 2 Estimates of covariate fixed-effect parameters for the final integrated model

Parameter		Definition	Value	RSE%	95% CI
Effects on acMMAE model parameters					
$CL_{INF, WT}$	θ_{22}	Weight effect on CL_{INF}	0.73	8.18	0.613–0.848
$V_{1,WT}$; $V_{2,WT}$; Q_{WT}	θ_{23}	Weight effect on V_1, V_2, and Q	0.50	6.24	0.439–0.561
$V_{1, males}$	θ_{24}	Male vs. female effect on V_1	1.20	1.83	1.16–1.24
$V_{1, ASIAN}$	θ_{25}	Asian race effect on V_1	0.929	4.18	0.852–1
$V_{1, NAÏVE}$	θ_{26}	Treatment-naive effect on V_1	1.2	1.96	1.16–1.25
$CL_{INF, SEX}$	θ_{27}	Sex effect on CL_{INF}	1.1	2.66	1.04–1.15
$CL_{INF, ALBUM}$	θ_{28}	Albumin effect on CL_{INF}	–0.247	36.3	–0.423 to –0.0712
$CL_{INF, RTX,Ob}$	θ_{29}	Combination therapy effect on CL_{INF}	0.844	2.95	0.795–0.892
$CL_{INF, B\text{-}cells}$	θ_{30}	B-cell count effect on CL_{INF}	0.0212	17.9	0.0138–0.0286
$CL_{INF,TMBD}$	θ_{31}	Tumor SPD effect on CL_{INF}	0.0521	27.4	0.0241–0.0801
$k_{des,NAÏVE}$	θ_{32}	Prior treatment effect on k_{des}	3.38	12.7	2.54–4.22
$K_{DES,RTX,Ob}$	θ_{33}	Combination therapy effect on k_{des}	0.932	11.2	0.727–1.14
$CL_{T,NAÏVE}$	θ_{34}	Treatment-naive effect on CL_T	3.53	34.7	1.13–5.93
$CL_{T,TMBD}$	θ_{35}	Tumor SPD of 50% effect on CL_T	1,150	46.0	114–2,190
$CL_{T,Threshold}$	θ_{36}	Threshold of B-cells on CL_T	121	46.0	11.9–229
$CL_{T,B\text{-}cells}$	θ_{37}	B-cell count effect on CL_T	0.578	24.6	0.3–0.856
Effects on acMMAE–MMAE relative conversion fraction					
$FRAC_{WT}$	θ_{38}	Weight effect on $FRAC_{NS}$	–0.467	23.1	–0.679 to –0.256
$FRAC_{SEX}$	θ_{39}	Sex effect on $FRAC_{NS}$	0.911	4.72	0.827–0.995
$FRAC_{NAIVE}$	θ_{40}	Treatment-naive status effect on $FRAC_{NS}$	0.756	5.95	0.668–0.844
$FRAC_{RTX,Ob}$	θ_{41}	Combination therapy effect on $FRAC_{NS}$	0.709	5.54	0.632–0.786
$FRAC_{HEPA}$	θ_{42}	Hepatic impairment on $FRAC_{NS}$	1.19	5.58	1.06–1.32
$FRAC_{ECOG}$	θ_{43}	ECOG PS (=0) effect on $FRAC_{NS}$	0.905	4.34	0.828–0.982
$FRAC_{ALB}$	θ_{44}	Albumin effect on $FRAC_{NS}$	–0.613	23.2	–0.892 to –0.334

ac, antibody-conjugated; CI, confidence interval; CL_{INF}, clearance at infinity; CL_t, linear time-dependent exponentially declining clearance; ECOG PS, Eastern Cooperative Oncology Group performance status; $FRAC_{NS}$, relative conversion fraction for nonspecific elimination; K_{des}, rate constant of CL_t decrease; MMAE, monomethyl auristatin E; PE, parameter estimate; RSE%, relative standard error (i.e., 100·SE/PE); SE, standard error; SPD, sum of the product of perpendicular dimensions. θ_{22} to θ_{44} symbols indicate fixed-effects parameters of the final model.

After pola 1.8 mg/kg q3w dosing, the percentage of acMMAE dose eliminated by CL_{NS} was 82.7% over cycle 1 and 95.2% over six cycles, suggesting that acMMAE PK is largely linear, consistent with the NCA results.[7] The initial value of CL_{NS} at time zero (= $CL_{INF} \times (1 + CL_{INF,EMAX})$) was 22.3% higher than the value at time of infinity (CL_{INF}). Estimated values of CL_{NS} were 1.01, 0.9, and 0.826 L/day (i.e., 0.0421, 0.0375, 0.0344 L/hour) at time zero, end of cycle 6, and infinity, respectively. The estimated T_{50} was 3.53 months (~5 cycles of q3w dosing).

Although playing a relatively minor role in the total clearance of acMMAE, CL_t significantly affected PK in the first cycle and contributed to a high IIV in cycle 1; CL_{MM} affected PK at low acMMAE concentrations across a range of pola doses and provided a better fitting of these data. Thus, both were justified and included in the model. CL_t declined exponentially with time (to zero value at infinity) as described by $CL_t = CL_T \times \exp(-k_{des} \times \text{time})$, where CL_T is the initial value, exp is exponential and k_{des} is the rate constant of exponential decline, with an estimated half-life of 6.28 days based on a k_{des} of 0.0046 hour^{-1}. Over cycle 1, 15.2% of the dose was eliminated by CL_t, with negligible elimination starting from cycle 2. At the therapeutic dose of 1.8 mg/kg, the CL_{MM} pathway played a negligible role, eliminating only 2% of the dose at each cycle (**Figure 2a**). The acMMAE central volume of distribution (V_1) was estimated as 3.15 L, which approximates the plasma volume.

PK exposures (assuming pola 1.8 mg/kg q3w) based on individual empirical Bayes estimates were simulated using the final model and summarized for the 460 patients in the analysis data set (**Table 3**). Coefficients of variation (CV% = mean/standard deviation × 100) for acMMAE AUC and C_{max} were 28.3% and 16.8%, respectively, for cycle 1, and 19.9% and 16.4%, respectively, for cycle 6.

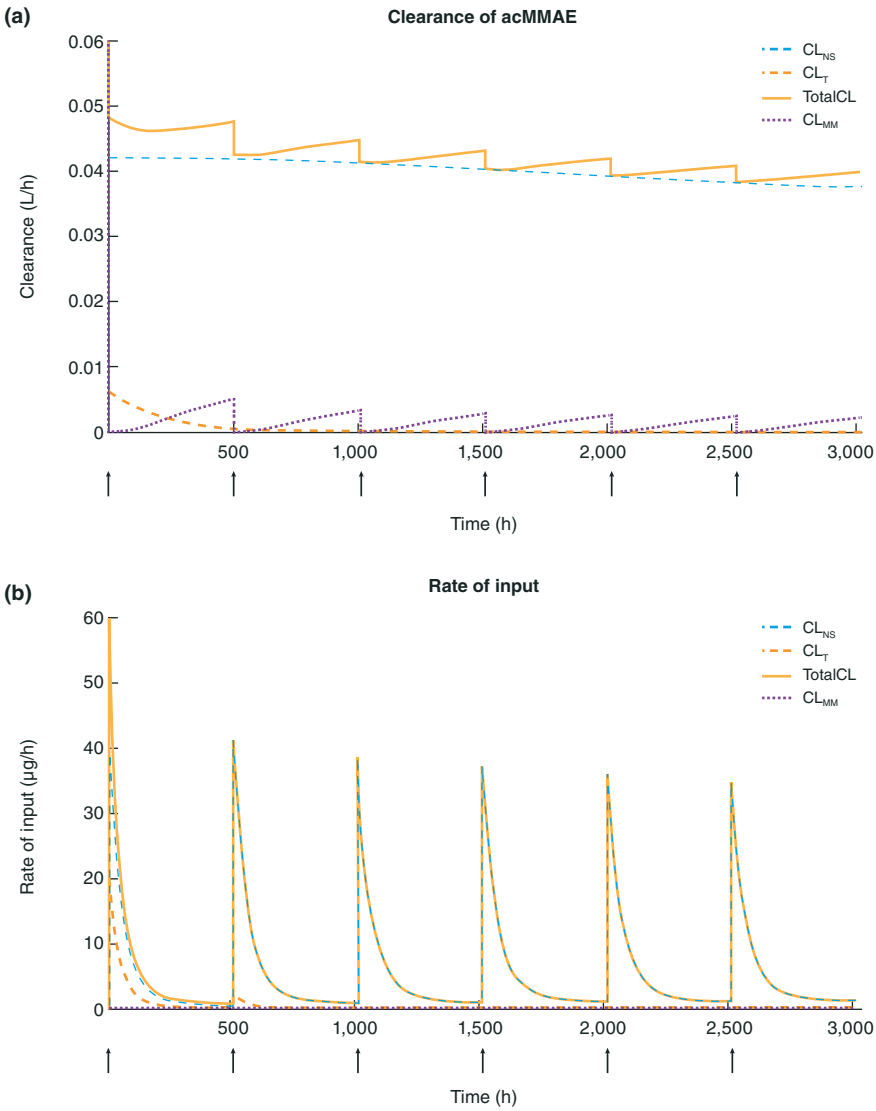

Figure 2 (**a**) Time-dependent change of clearance of acMMAE and (**b**) time-dependent change of input rate (µg/hour) to unconjugated MMAE central compartment due to acMMAE catabolism after repeated q3w dosing. In **a**, simulation is based on PK parameters of a typical patient assuming pola 1.8 mg/kg q3w dosing (bodyweight = 80 kg and MMAE equivalent dose = 2,600 µg). In **b**, each input rate is the product of clearance, the relative fraction of formation, and acMMAE concentration (Eq. 2). Black arrows indicate pola dosing times at 0, 504, 1,008, 1,512, 2,016, and 2,520 hours (i.e., q3w for six cycles). ac, antibody-conjugated; CL_{NS}, nonspecific time-dependent linear clearance; CL_{MM}, Michaelis–Menten clearance; CL_{NS}_Input, input rate from the CL_{NS} pathway; CL_t, linear time-dependent exponentially declining clearance; CL_T_Input, input rate from the CL_t pathway; MMAE, monomethyl auristatin E; MM_Input, input rate from the Michaelis–Menten pathway; PK, pharmacokinetic; pola, polatuzumab vedotin; q3w, once every 3 weeks; Total CL, total clearance (i.e., the sum of CL_{NS}, CL_t, and CL_{MM}); Total_Input, CL_{NS}_Input + CL_T_Input + MM_Input.

The highly variable CL_T (IIV, 138%) mainly at cycle 1 may have contributed to a slightly larger PK variability at cycle 1 than at cycle 6. The acMMAE terminal half-life ($t_{1/2,terminal}$) was approximately 12 days (95% CI 8.1–19.5 days, $N = 460$) at cycle 6 based on the popPK model, which is longer than the cycle 1 $t_{1/2,terminal}$ based on an NCA of 5–6 days[7] as a result of the different estimation method and time-dependent decrease of acMMAE clearance on repeated dosing. The cycle 6 half-life was the longest for the planned six cycles of dosing, which is the most conservative and was used to estimate the contraception duration of 3 months (in the US label) after the final dose for females of reproductive potential.[14]

The acMMAE AUC and trough concentration (C_{trough}) increased moderately with repeated q3w dosing (**Table 3**), potentially as a result of the decrease of acMMAE clearance with time. There was no apparent increase in C_{max} values. Following pola 1.8 mg/kg q3w dosing, 30%, 3%, and 81% increases in acMMAE AUC, C_{max}, and C_{trough} were predicted at cycle 3 over cycle 1, with achievements of 91%, 99%, and 81% of the cycle 6 AUC, C_{max}, and C_{trough}, respectively. Cycle 6 AUC, the theoretically maximum AUC for the

Table 3 Predicted mean ± SD (CV%) of acMMAE and unconjugated MMAE exposures by cycle based on individual EBE parameters (estimated based on individual covariate values) assuming 1.8 mg/kg q3w dosing

	acMMAE			Unconjugated MMAE		
Cycle	AUC, ng × day/mL, (%)	C_{max}, ng/mL, (%)	C_{trough}, ng/mL, (%)	AUC, ng × day/mL, (%)	C_{max}, ng/mL, (%)	C_{trough}, ng/mL, (%)
1	2,020 ± 571 (28.3)	690 ± 116 (16.8)	13.1 ± 6.58 (50.2)	36.5 ± 33.9 (92.9)	4.08 ± 3.99 (97.8)	0.269 ± 0.820 (305)
3	2,640 ± 522 (19.8)	713 ± 117 (16.4)	23.7 ± 10.1 (42.6)	26.4 ± 24.5 (92.8)	2.45 ± 1.83 (74.7)	0.302 ± 0.707 (234)
6	2,900 ± 577 (19.9)	721 ± 118 (16.4)	29.3 ± 12.3 (42.0)	25.1 ± 19.6 (78.1)	2.27 ± 1.57 (69.2)	0.308 ± 0.527 (171)
30[a]	3,220 ± 645 (20.0)	730 ± 118 (16.2)	36.5 ± 15.0 (41.1)	23.0 ± 17.8 (77.4)	2.02 ± 1.40 (69.3)	0.309 ± 0.479 (155)

ac, antibody-conjugated; AUC, area under the concentration-time curve; C_{max}, maximum concentration; C_{trough}, trough concentration; CV, coefficient of variation; EBE, empirical Bayes estimate; MMAE, monomethyl auristatin E; q3w, once every 3 weeks; SD, standard deviation.
[a]Represents hypothetical steady-state exposures after repeated dosing to time of infinity.

proposed dosing regimen of up to six cycles, was approximately 40% above cycle 1 AUC. Cycle 6 AUC, C_{max}, and C_{trough} achieved 90%, 99%, and 80% of theoretical steady-state values (represented by the simulated exposure values at cycle 30 after hypothetical repeated q3w dosing, at which time the CL_{NS} approximated the value at infinity (CL_{INF})).

Covariates impacting acMMAE PK

In the final model, baseline bodyweight, sex, serum albumin level, B-cell count, tumor sum of the product of perpendicular dimensions, and coadministration of rituximab/obinutuzumab (R/G) (vs. single-agent therapy) were statistically significant covariates (P = 0.01) for CL_{INF} (i.e., the nonspecific linear clearance pathway). Being male, higher bodyweight, B-cell counts and baseline tumor sum of the product of perpendicular dimensions, lower albumin, and single-agent pola treatment were associated with faster CL_{INF}; and being male, higher bodyweight, non-Asian race, and treatment-naive status were associated with higher V_1.

The IIV in acMMAE CL_{INF} and V_1 was low. The CV% of IIV in acMMAE CL_{INF} and V_1 were 28.8% and 22.6%, respectively, in the base model, and were reduced to 19.5% and 12.2%, respectively, in the final model after accounting for all statistically significant covariates. Bodyweight explained 36.1% and 43.1% of the IIV (ω^2) in CL_{INF} and V_1, respectively, as computed by the percent difference of the base model and an interim model with bodyweight as the only covariate on model parameters. All covariates together (the final model) explained 54.2% and 70.6% of IIV (ω^2) in CL_{INF} and V_1, respectively, compared with the base model. Bodyweight-based dosing was expected to provide lower PK exposure variability than a hypothetical flat dosing based on the power coefficient for the effect of bodyweight of 0.73 for the CL_{INF} of acMMAE, which is closer to one than zero (**Table 2**).[29]

The sensitivity analysis suggested that, given the bodyweight-based dosing, the magnitude of the impact of extreme values of bodyweight (i.e., 2.5th and 97.5th percentiles) was < 25% on C_{max} and < 13% on AUC when compared with a typical patient with median bodyweight, whereas all other statistically significant covariates had an even small magnitude of impact on acMMAE exposures (<20% for both AUC and C_{max}; **Figure 3a,b**). These differences were relatively close to the CV% of acMMAE C_{max} and AUC (16% and 20%, respectively, at cycle 6; **Table 3**) and were not expected to have a clinically meaningful impact on efficacy and safety. Overall, bodyweight-based dosing is supported, and further dose adjustment based on other covariates is not warranted.

PopPK of unconjugated MMAE

As a catabolite of acMMAE, the final model (**Figure 1**) suggested that CL_{NS}, CL_t and CL_{MM} of acMMAE provided inputs to unconjugated MMAE formation. The relative fraction of formation from the CL_{NS}, CL_t and CL_{MM} pathways is $FRAC_{NS}$, $FRAC_{NS} \times FRAC_{CLT}$ ($FRAC_{CLT}$ = 3.70), and $FRAC_{NS} \times FRAC_{MM}$ ($FRAC_{MM}$ = 2.72), respectively. The unconjugated MMAE exposures decreased with time based on observed PK data with relatively dense sampling during the first four cycles (Genentech, data on file), which was modeled by the time-dependent change of total input rate (μg/hour) on repeated dosing (Eq. 2).

$$\text{Total input rate} = \left(FRAC_{NS} \times FRAC_{CLT} \times CL_T \times \frac{\exp(-k_{des} \times \text{time})}{V_1} + FRAC_{NS} \times CL_{INF} \times \frac{\left(1 + CL_{INF,EMAX} \times \frac{T_{50}^{\gamma}}{T_{50}^{\gamma} + \text{time}^{\gamma}}\right)}{V_1} + FRAC_{NS} \times FRAC_{MM} \times \frac{V_{MAX}}{\left(K_M + \frac{A(1)}{V_1}\right)} \right) \times A(1) \quad (2)$$

A(1) represents the amount of acMMAE in the central compartment; all other parameters are listed in **Table 1**.

In Eq. 2, $FRAC_{NS} = FRAC_{INF}\,(1 + FRAC_T \times e^{-\alpha \times \text{time}})$, where $FRAC_{INF}$ = 1 and $FRAC_T$ is the initial time-dependent part of $FRAC_{NS}$. The declining half-life was estimated to be 4.2 months (α = 0.167 month^{-1}) with an initial value 13.9% higher than the value at infinity. Based on Eq. 2, a combination of three factors, including time-dependent changes in acMMAE clearances, changes in acMMAE concentrations in the central compartment with mild accumulation at later cycles as a result of repeated dosing, and a time-dependent decrease of $FRAC_{NS}$, resulted in a time-dependent change in the total input rate on repeated dosing (**Figure 2b**). A gradual decrease in the area under the input rate–time curve for each cycle was apparent, which represents the cumulative amount of input to form unconjugated MMAE within each cycle. The biggest decrease occurred from cycle 1 to cycle 2, suggesting that the input from the CL_t pathway plays a major role in the dynamics of time-dependent decrease of cumulative input. This model described the

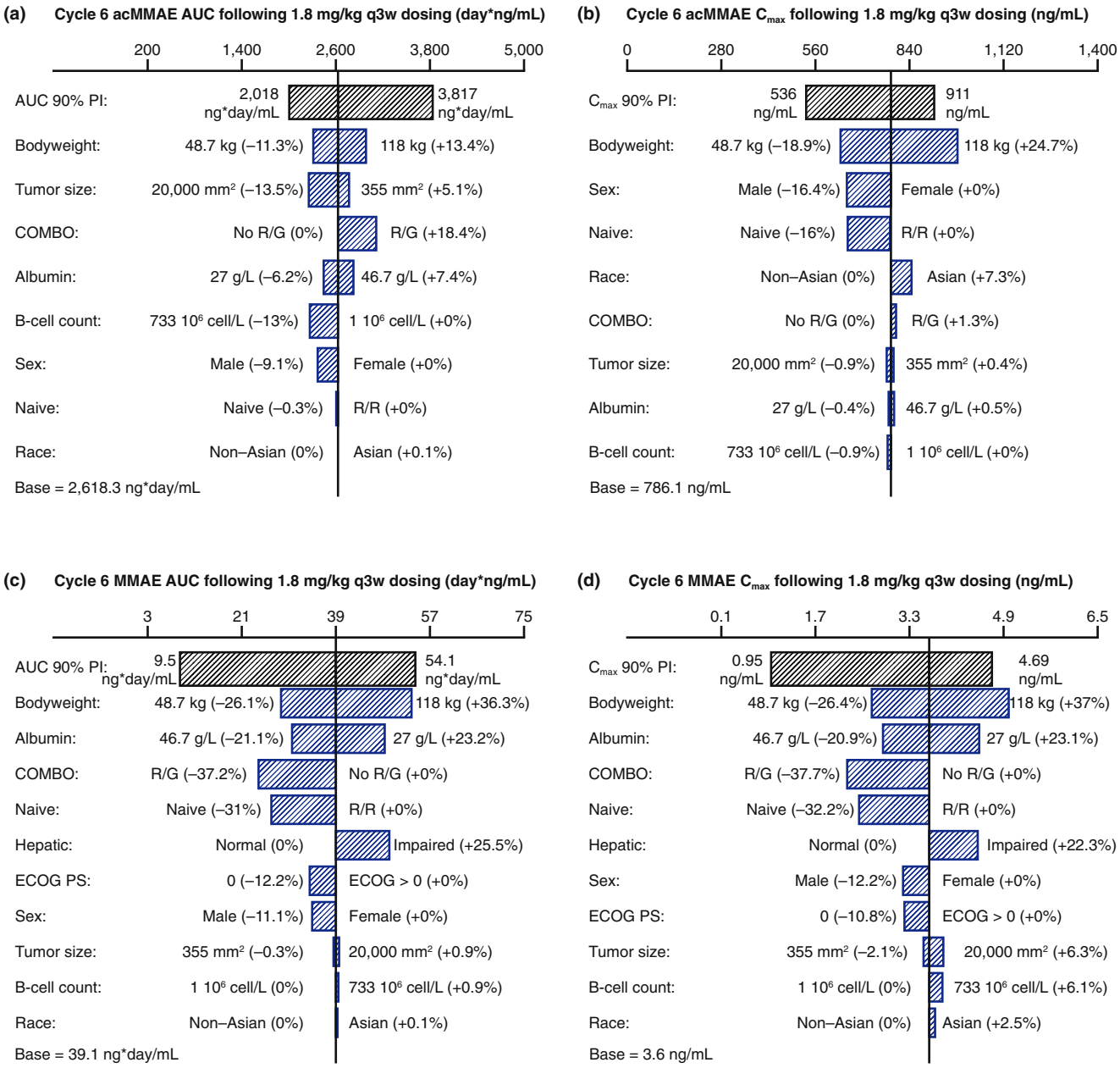

Figure 3 Sensitivity analysis evaluating the impact of covariates on cycle 6 acMMAE (**a**) AUC and (**b**) C_{max} and on cycle 6 unconjugated MMAE (**c**) AUC and (**d**) C_{max}. Base, as represented by the black vertical line and red values, refers to the predicted cycle 6 exposure (AUC or C_{max}) of acMMAE or unconjugated MMAE in a typical patient. The black shaded bar shows the minimum and maximum exposure range across the entire population based on individual predictions. Each blue shaded bar represents the influence of a single covariate on the cycle 6 exposure after repeated pola dosing at 1.8 mg/kg q3w. The label at the left end of the bar represents the covariate being evaluated. The length of each bar describes the potential impact of that particular covariate on acMMAE or unconjugated MMAE exposure at cycle 6, with the percentage value in the parentheses at each end representing the percent change in exposure from the base. ac, antibody-conjugated; AUC, area under the concentration-time curve; C_{max}, maximum concentration; COMBO, combination; ECOG ps, Eastern Cooperative Oncology Group performance status; G, obinutuzumab; MMAE, monomethyl auristatin E; 90% PI, 5th% to 95th% prediction interval; q3w, once every 3 weeks; R, rituximab; R/R, relapsed/refractory.

time-dependent decrease of unconjugated MMAE AUC and C_{max} of each cycle on repeated dosing (**Table 3**), which is consistent with observed data. A similar magnitude of decrease (cycles 2 and 3 AUC and C_{max} were 50 – 80% of cycle 1 values) was observed for brentuximab vedotin.[30]

The systemic PK of unconjugated MMAE was described by a two-compartment model. Two clearance pathways, including linear and nonlinear MM pathways, contributed to unconjugated MMAE elimination from the central compartment. The apparent clearance for the linear pathway (CL_{MMAE}), which is the ratio of systemic clearance to actual fraction of formation, was estimated to be 1.89 L/hour. The unconjugated MMAE elimination is unlikely to be nonlinear. Given the formation-rate-limited kinetics of unconjugated

MMAE, the nonlinear MM elimination may actually reflect the nonlinearity of unconjugated MMAE formation.

Simulation of PK exposures based on individual empirical Bayes estimates of PK parameters demonstrated CV% values for unconjugated MMAE AUC and C_{max} of 92.9% and 97.8%, respectively, at cycle 1, and 78.1% and 69.2%, respectively, at cycle 6 (**Table 3**). Thus, the variabilities of unconjugated MMAE exposures were much larger than acMMAE, likely because of the variability in the formation of unconjugated MMAE as a catabolite of acMMAE. With pola 1.8 mg/kg q3w dosing, AUC and C_{max} values for unconjugated MMAE were the highest in cycle 1, declining to approximately 72% and 60% of cycle 1 values, respectively, at cycle 3 and 69% and 56% of cycle 1 values, respectively, at cycle 6. The majority of the decreases occurred before cycle 3, with >67% and >75% of the overall decrease occurring during cycles 2 and 3. A slight increase in C_{trough} was observed at cycle 3 vs. cycle 1 (12% higher; **Table 3**), but was not considered clinically meaningful given the overall low C_{trough} values (<0.5 ng/mL) and large PK variability.

Covariates impacting unconjugated MMAE PK

In the final model, baseline values for bodyweight, sex, serum albumin level, R/G combination treatment, previously untreated status, hepatic function based on the National Cancer Institute Organ Dysfunction Working Group Classification,[31] and Eastern Cooperative Oncology Group performance status were identified as statistically significant covariates for $FRAC_{NS}$ (**Table 2**). Specifically, being male, higher bodyweight, higher albumin levels, receipt of R/G combination therapy, treatment naïve, normal hepatic function, and Eastern Cooperative Oncology Group performance status 0 (vs. ≥1) were associated with a lower $FRAC_{NS}$ (or potentially higher systemic clearances). As unconjugated MMAE is a catabolite of pola, it is likely that these covariates might impact the fraction of formation or systemic clearances of unconjugated MMAE or a combination of both. For modeling simplicity, all covariates were added to the parameter of relative fraction of formation rather than the systemic parameters of unconjugated MMAE.

The sensitivity analysis suggested that higher bodyweight, lower albumin levels, impaired hepatic function, receipt of single-agent treatment, and R/R status were associated with a moderate increase (approximately 20–40%) in unconjugated MMAE exposures (AUC and C_{max}) compared with a reference patient (**Figure 3c,d**), with bodyweight having the largest impact. However, the magnitudes of impact of these covariates were relatively small when compared with the CV% of unconjugated MMAE C_{max} and AUC (69.2% and 78.1%, respectively, at cycle 6; **Table 3**) and were not expected to have a clinically meaningful impact on safety (Genentech data on file).

DISCUSSION AND CONCLUSIONS

The integrated acMMAE–MMAE popPK model reported here is the first integrated popPK model to describe the PK of antibody-conjugated and unconjugated payload together with covariate assessments for each analyte. Historically, integrated models for multiple analytes of MMAE-containing ADCs focused either on Tab–acMMAE[15,16] or ADC–unconjugated MMAE.[32] Because acMMAE represents MMAE conjugated to the antibody, although the ADC represents antibody that is conjugated to MMAE, acMMAE and ADC have slightly different PK properties. The ADC-unconjugated MMAE model developed for brentuximab vedotin,[32] an ADC with the identical linker, payload and conjugation sites as pola, is not applicable for pola because of the different analytes of the conjugate that were included in each model.

Three clearance pathways were identified for acMMAE, which is aligned with the mechanistic understanding of ADC disposition targeting B cells. Hypothetically, multiple pathways contribute to acMMAE disposition, including systemic/extracellular disposition, tissue disposition and binding, and intracellular disposition and a bystander effect (**Figure 4**). The systemic/extracellular process (**Figure 4a**) might involve deconjugation extracellularly and is a nonspecific pathway.[15] The tissue disposition and binding (**Figure 4b**) are followed by intracellular disposition involving cellular uptake, intracellular degradation by protease enzymes and a subsequent bystander effect (**Figure 4c**). Nonspecific and target-mediated pathways contribute to these processes. The nonspecific pathways, including phagocytosis, pinocytosis, fragment crystallizable neonatal receptor-mediated or fragment crystallizable gamma receptor-mediated cellular uptake and intracellular degradation, similar to typical mAbs, are expected to play a major role compared with the target-mediated pathway given the largely linear PK of acMMAE; the target-mediated pathway driven by binding to CD79b on B cells is expected to play a relatively minor role at clinical doses.

Among the three clearance pathways in the model, the CL_{NS} pathway may reflect a combination of all nonspecific pathways described previously. The slow decline from 1.01 L/day at time zero to 0.9 L/day at the end of cycle 6 might be correlated with an overall improvement in patient health status (as a result of effective treatment or other reasons). This has also been reported for other mAbs, such as nivolumab,[33] pembrolizumab,[34] and atezolizumab.[35] Both the CL_t and CL_{MM} pathways may be related to target-mediated clearances. The CL_t pathway that exponentially declined to zero beyond the first cycle may reflect a rapid elimination of target-expressing cells by pola in highly perfused organs; the CL_t pathway contributes to a large IIV of cycle 1 acMMAE exposures. The presence of a rapidly decreased clearance pathway in addition to the linear nonspecific clearance is also identified for other MMAE ADCs binding to different targets[16] and for mAbs targeting diffusive/circulating targets such as B cells (e.g., rituximab[36] and obinutuzumab[17]). The CL_{MM} pathway played a negligible role in the total clearance at the pola dose of 1.8 mg/kg, but greatly improved the model fitting to low acMMAE concentrations.

The three clearance pathways of acMMAE provided separate input for unconjugated MMAE formation. Given the complex disposition of an ADC, unconjugated MMAE is the major catabolite[37] and the only catabolite quantified in patients' systemic circulation given its clinical relevance in

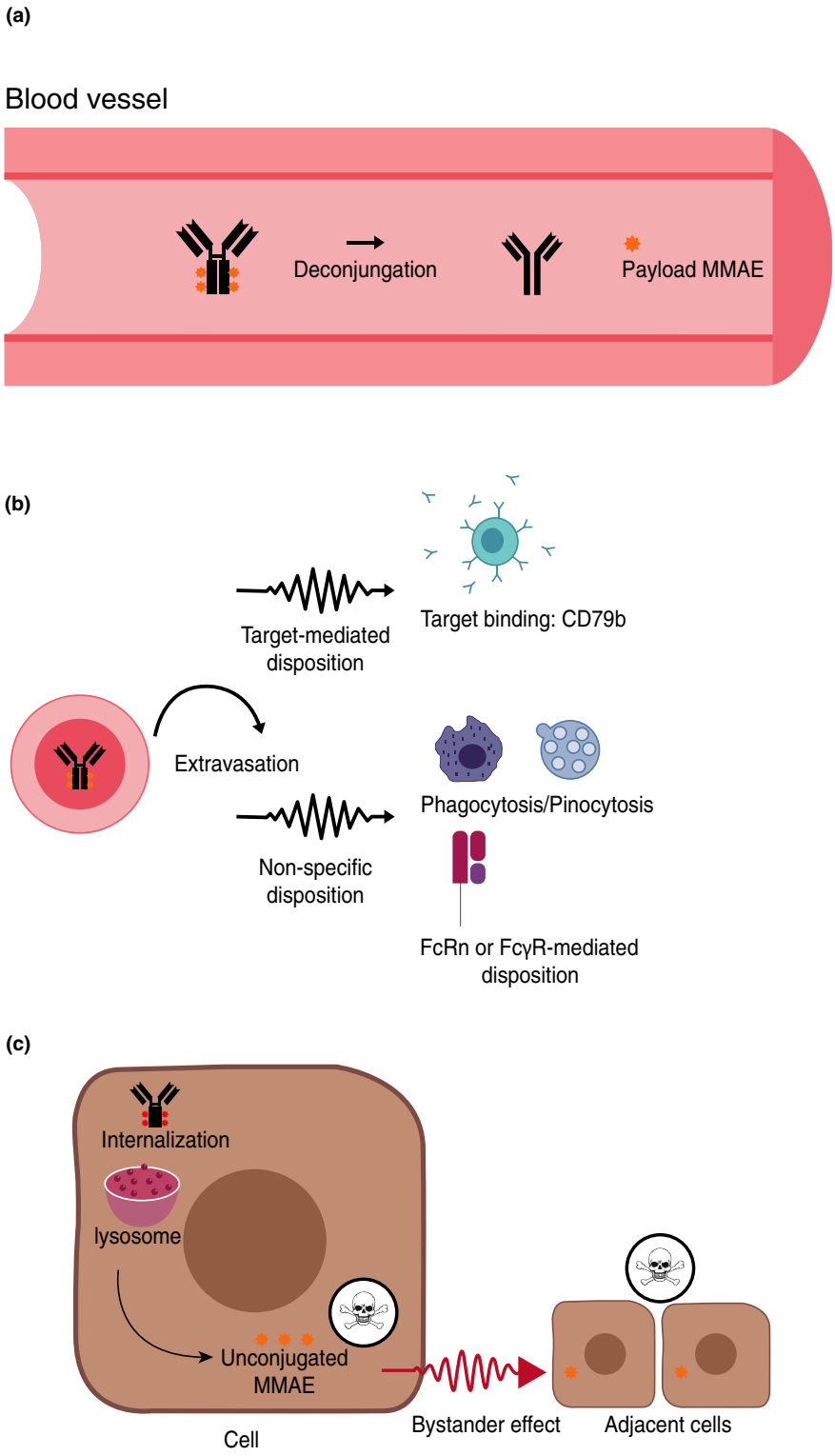

Figure 4 Hypothetical schema describing the disposition of pola after intravenous administration (**a**) systemic/extracellular disposition, (**b**) tissue disposition and binding, and (**c**) intracellular disposition after cellular uptake and subsequent bystander effect. In **c**, the sizes of the cell with internalized conjugate and adjacent cells are for illustration only and do not reflect a real size difference. FcRn, fragment crystallizable neonatal receptor; FcγR, fragment crystallizable gamma receptor; MMAE, monomethyl auristatin E.

pola clinical studies. Based on NCA, the cycle 1 values of $t_{1/2,terminal}$ for unconjugated MMAE and acMMAE were similar (approximately 4 and 5–6 days, respectively),[7] suggesting formation-rate limited kinetics of unconjugated MMAE. As it is impossible to directly obtain PK data for intravenous administration of unconjugated MMAE in patients because

of its high toxicity, the absolute fraction of formation from acMMAE to unconjugated MMAE cannot be estimated, and only the apparent clearance and volume of distribution of unconjugated MMAE (i.e., the ratio between the true value and absolute fraction of formation) can be estimated. The relative fractions of formation from the CL_t and CL_{MM} pathways ($FRAC_{CLT}$ and $FRAC_{MM}$) are estimated to be 3.7-fold and 2.72-fold of the CL_{NS} pathway ($FRAC_{NS}$), respectively (**Table 1**), whereas the clearance value is higher for the CL_{NS} than the CL_t and CL_{MM} pathways (**Figure 2a**). The input rate for each clearance pathway is related to the product of relative fraction of formation and clearance (equation 2), with the CL_{NS} pathway playing a major role (**Figure 2b**). Mechanistically, CL_t and CL_{MM} are potentially related to target-mediated clearance by malignant B cells in NHL patients, which are easily accessible by systemic circulation through the lymphatic system. This may explain the higher relative fraction of formation of systemic MMAE from these two pathways when compared with the formation from the CL_{NS} pathway. The CL_{NS} pathway involves tissues in the whole body, including the liver that may catabolize acMMAE and excrete unconjugated MMAE to bile without going back to the systemic circulation, or involves chemical reactions such as deconjugation by maleimide exchange[38] that potentially generate MMAE-related catabolites that may not account for systemic MMAE formation. Relative contributions of the three acMMAE elimination pathways differ in time and concentration regions and thus impact the kinetics of unconjugated MMAE input rate (**Figure 2a,b**): CL_t plays a significant role only in the first cycle, CL_{MM} mainly contributes to acMMAE elimination at low concentrations, while CL_{NS} is important across cycles and slowly decreases with time. These differences allowed the parameter identifiability and successful parameter estimation with high precision for $FRAC_{NS}$, $FRAC_{CLT}$, and $FRAC_{MM}$.

As unconjugated MMAE is a catabolite of acMMAE, the covariates impacting acMMAE PK can affect unconjugated MMAE PK, but not vice versa. The sequential covariate analysis approach enabled the identification of covariates that affect only unconjugated MMAE PK (step 4) based on further reduction of IIV estimates of MMAE PK parameters on top of the model with covariates identified for acMMAE PK (step 3). As a result, some covariates impact both analytes, whereas others are unique for each analyte (**Table 2**). For example, higher bodyweight is correlated with both faster acMMAE CL_{NS} and lower $FRAC_{NS}$ of unconjugated MMAE (or potentially higher CL_{MMAE}), and both factors can affect unconjugated MMAE exposures. In contrast, hepatic impairment is correlated with higher $FRAC_{NS}$ (or potentially lower CL_{MMAE} or both), but it does not affect acMMAE PK. All parameters related to the effects of covariates on both analytes were estimated with good precision, confirming the identifiability of model parameters.

In summary, this analysis supports the concept that acMMAE PK is mainly driven by its antibody component, largely linear with CL_{NS} as the major clearance pathway across cycles. A mild accumulation of acMMAE after q3w dosing was observed, which was potentially the result of the time-dependent decrease of clearance. cycle 3 acMMAE AUC increased by approximately 30% over cycle 1 AUC, and achieved >90% of the cycle 6 AUC. The acMMAE half-life at cycle 6 was approximately 12 days (95% CI, 8.1–19.5 days) with predicted CL_{NS} of 0.9 L/day. Unconjugated MMAE plasma exposures appeared following formation-rate limited kinetics, with its exposure much lower than acMMAE exposures and with higher IIV. There was a time-dependent decrease of input amount per cycle for MMAE formation, which described the decreased unconjugated MMAE exposures after repeated dosing. The model was further applied to support bodyweight-based dosing and to justify clinical dose in subgroups of patients, which will be reported separately.

Supporting Information. Supplementary information accompanies this paper on the *CPT: Pharmacometrics & Systems Pharmacology* website (www.psp-journal.com).

Supplementary Information – Nonlinear Mixed-Effect Modeling (NONMEM) code, Equations, Tables S1–S3, and Figures S1–S3

Acknowledgments. We thank the patients and their families who participated in the polatuzumab vedotin clinical trials, without whom this study would not have been possible. We acknowledge and thank the investigators and site staff. Medical writing support was provided by Emma McConnell and Andrea Bothwell of Gardiner-Caldwell Communications and was funded by F. Hoffmann-La Roche Ltd.

Funding. This study was funded by F. Hoffmann-La Roche Ltd.

Conflict of Interest. All authors, except Leonid Gibiansky, are employees of Genentech, Inc. and stockholders of the Roche group. Leonid Gibiansky is a paid consultant for Roche and Genentech.

Author Contributions. All authors wrote the manuscript. D.L., R.C.D., C.L., D.M., and J.H. designed the research. D.L., T.L., X.L., R.C.D., P.A. performed the research. D.L., T.L., L.G. analyzed the data.

Data Availability Statement. Qualified researchers may request access to individual patient level data through the clinical study data request platform (www.clinicalstudydatarequest.com). Further details on Roche's criteria for eligible studies are available here (https://clinicalstudydatarequest.com/Study-Sponsors/Study-Sponsors-Roche.aspx). For further details on Roche's Global Policy on the Sharing of Clinical Information and how to request access to related clinical study documents, see here (https://www.roche.com/research_and_development/who_we_are_how_we_work/clinical_trials/our_commitment_to_data_sharing.htm).

1. Dornan, D. *et al.* Therapeutic potential of an anti-CD79b antibody-drug conjugate, anti-CD79b-vc-MMAE, for the treatment of non-Hodgkin lymphoma. *Blood* **114**, 2721–2729 (2009).
2. Abdollahpour-Alitappeh, M. *et al.* Monomethyl auristatin E, a potent cytotoxic payload for development of antibody-drug conjugates against breast cancer. *Novel Biomed.* **5**, 98–103 (2017).
3. Lu, D. *et al.* Time-to-event analysis of polatuzumab vedotin-induced peripheral neuropathy to assist in the comparison of clinical dosing regimens. *CPT Pharmacometrics Syst. Pharmacol.* **6**, 401–408 (2017).
4. Niemann, C.U. & Wiestner, A. B-cell receptor signaling as a driver of lymphoma development and evolution. *Semin. Cancer Biol.* **23**, 410–421 (2013).
5. Lu, J., Jiang, F., Lu, A. & Zhang, G. Linkers having a crucial role in antibody-drug conjugates. *Int. J. Mol. Sci.* **17**, 561 (2016).
6. Doronina, S.O. *et al.* Development of potent monoclonal antibody auristatin conjugates for cancer therapy. *Nat. Biotechnol.* **21**, 778–784 (2003).
7. Palanca-Wessels, M.C. *et al.* Safety and activity of the anti-CD79B antibody-drug conjugate polatuzumab vedotin in relapsed or refractory B-cell non-Hodgkin lymphoma and chronic lymphocytic leukaemia: a phase 1 study. *Lancet Oncol.* **16**, 704–715 (2015).

8. Matasar, M. *et al.* Polatuzumab vedotin plus bendamustine and rituximab or obinutuzumab in relapsed/refractory FL or DLBCL: updated results of a phase 1b/2 study. *Hematol. Oncol.* **35**(suppl. 2), 271–272 (2017).
9. Matasar, M. *et al.* Polatuzumab vedotin plus bendamustine and rituximab or obinutuzumab in relapsed/refractory follicular lymphoma or diffuse large B-cell lymphoma: updated results of a phase 1b/2 study. *Haematologica* **102**(suppl. 2), 173 (2017).
10. Tilly, H. *et al.* Polatuzumab vedotin in combination with immunochemotherapy in patients with previously untreated diffuse large B-cell lymphoma: an open-label, non-randomised, phase 1b–2 study. *Lancet Oncol.* **20**, 998–1010 (2019).
11. Morschhauser, F. *et al.* Polatuzumab vedotin or pinatuzumab vedotin plus rituximab in patients with relapsed or refractory non-Hodgkin lymphoma: final results from a phase 2 randomised study (ROMULUS). *Lancet Haematol.* **6**, e254–e265 (2019).
12. Phillips, T. *et al.* Polatuzumab vedotin combined with obinutuzumab for patients with relapsed or refractory non-Hodgkin lymphoma: preliminary safety and clinical activity of a phase Ib/II study. *Blood* **128**, 622 (2016).
13. Sehn, L.H. *et al.* Randomized phase 2 trial of polatuzumab vedotin (pola) with bendamustine and rituximab (BR) in relapsed/refractory (r/r) FL and DLBCL. *J. Clin. Oncol.* **36**(15 suppl.), 7507 (2018).
14. Highlights of prescribing information: POLIVY™ (polatuzumab vedotin-piiq) for injection, for intravenous use. Initial US Approval: 2019 <https://www.accessdata.fda.gov/drugsatfda_docs/label/2019/761121s000lbl.pdf> (2019). Accessed June 18, 2019.
15. Lu, D. *et al.* Integrated two-analyte population pharmacokinetic model for antibody-drug conjugates in patients: implications for reducing pharmacokinetic sampling. *CPT Pharmacometrics Syst. Pharmacol.* **5**, 665–673 (2016).
16. Kagedal, M. *et al.* Platform model describing pharmacokinetic properties of vc-MMAE antibody-drug conjugates. *J. Pharmacokinet. Pharmacodyn.* **44**, 537–548 (2017).
17. Gibiansky, E., Gibiansky, L., Carlile, D.J., Jamois, C., Buchheit, V. & Frey, N. Population pharmacokinetics of obinutuzumab (GA101) in chronic lymphocytic leukemia (CLL) and non-Hodgkin's lymphoma and exposure-response in CLL. *CPT Pharmacometrics Syst. Pharmacol.* **3**, e144 (2014).
18. Gorovits, B. *et al.* Bioanalysis of antibody-drug conjugates: American Association of Pharmaceutical Scientists Antibody-Drug Conjugate Working Group position paper. *Bioanalysis.* **5**, 997–1006 (2013).
19. Kaur, S., Xu, K., Saad, O.M., Dere, R.C. & Carrasco-Triguero, M. Bioanalytical assay strategies for the development of antibody-drug conjugate biotherapeutics. *Bioanalysis.* **5**, 201–226 (2013).
20. Lu, D. *et al.* Population pharmacokinetics and exposure-response assessment of anti-CD79b antibody drug conjugate (ADC) (polatuzumab vedotin) in relapsed/refractory B-cell lymphoma patients: interim analysis results. *Clin. Pharmacol. Ther.* **97**(suppl. 1), S60–S96 (2015).
21. R Foundation for Statistical Computing. R: A Language and Environment for Statistical Computing (R Foundation for Statistical Computing, Vienna, Austria, 2018) <http://www.r-project.org/>. Accessed March 6, 2019.
22. Bergstrand, M. *et al.* Prediction-corrected visual predictive checks for diagnosing nonlinear mixed-effects models. *AAPS J.* **13**, 143–151 (2011).
23. Brendel, K. *et al.* Metrics for external model evaluation with an application to the population pharmacokinetics of gliclazide. *Pharm. Res.* **23**, 2036–2049 (2006).
24. Mentré, F. *et al.* Prediction discrepancies for the evaluation of nonlinear mixed-effects models. *J. Pharmacokinet. Pharmacodyn.* **33**, 345–367 (2006).
25. Gastonguay, M.R. A full model estimation approach for covariate effects: inference based on clinical importance and estimation precision. *AAPS J.* **6**(suppl. 1), abstract W4354 (2004).
26. Gastonguay, M.Full covariate models as an alternative to methods relying on statistical significance for inferences about covariate effects: a review of methodology and 42 case studies <https://www.page-meeting.org/?abstract=2229> (2011).
27. Bergstrand, M. & Karlsson, M.O. Handling data below the limit of quantification in mixed effect models. *AAPS J.* **11**, 371–380 (2009).
28. Beal, S.L. Ways to fit a PK model with some data below the quantification limit. *J Pharmacokinet. Pharmacodyn.* **28**, 481–504 (2001).
29. Bai, S. *et al.* A guide to rational dosing of monoclonal antibodies. *Clin. Pharmacokinet.* **51**, 119–135 (2012).
30. Center for Drug Evaluation and Research. Clinical pharmacology and biopharmaceutics reviews: BLA 125388 & 125399–brentuximab vedotin <https://www.accessdata.fda.gov/drugsatfda_docs/nda/2011/125388Orig1s000ClinPharmR.pdf> (2011). Accessed May 24, 2019.
31. Ramalingam, S.S. *et al.* Phase I study of vorinostat in patients with advanced solid tumors and hepatic dysfunction: a National Cancer Institute Organ Dysfunction Working Group study. *J. Clin. Oncol.* **28**, 4507–4512 (2010).
32. Li, H., Han, T.H., Hunder, N.N., Jang, G. & Zhao, B. Population pharmacokinetics of brentuximab vedotin in patients with CD30-expressing hematologic malignancies. *J. Clin. Pharmacol.* **57**, 1148–1158 (2017).
33. Nivolumab PI <https://www.accessdata.fda.gov/drugsatfda_docs/label/2019/125554s073lbl.pdf>. Accessed September 11, 2019.
34. Pembrolizumab PI <https://www.accessdata.fda.gov/drugsatfda_docs/label/2019/125514s055s056lbl.pdf>. Accessed September 11, 2019.
35. Atezolizumab PI <https://www.accessdata.fda.gov/drugsatfda_docs/label/2019/761034s014lbl.pdf>. Accessed 11 September 2019.
36. Rozman, S., Grabnar, I., Novakovic, S., Mrhar, A. & Jezersek Novakovic, B. Population pharmacokinetics of rituximab in patients with diffuse large B-cell lymphoma and association with clinical outcome. *Br. J. Clin. Pharmacol.* **83**, 1782–1790 (2017).
37. Han, T.H. *et al.* CYP3A-mediated drug-drug interaction potential and excretion of brentuximab vedotin, an antibody-drug conjugate, in patients with CD30-positive hematologic malignancies. *J. Clin. Pharmacol.* **53**, 866–877 (2013).
38. Shen, B.Q. *et al.* Conjugation site modulates the in vivo stability and therapeutic activity of antibody-drug conjugates. *Nat. Biotechnol.* **30**, 184–189 (2012).